Solar Wind Interaction and Pressure Balance at the Dayside Ionopause of Mars

Feng Chu[1], Firdevs Duru[2], Zachary Girazian[3], Robin Ramstad[4], Jasper S. Halekas[5], Donald A. Gurnett[5], Xin Cao[5], and Andrew J. Kopf[5]

[1]Los Alamos National Laboratory
[2]Coe College
[3]The University of Iowa
[4]University of Colorado Boulder
[5]University of Iowa

November 26, 2022

Abstract

Due to the lower ionospheric thermal pressure and existence of the crustal magnetism at Mars, the Martian ionopause is expected to behave differently from the ionopause at Venus. We study the solar wind interaction and pressure balance at the ionopause of Mars using both in situ and remote sounding measurements from the MARSIS (Mars Advanced Radar for Subsurface and Ionosphere Sounding) instrument on the Mars Express orbiter. We show that the magnetic pressure usually dominates the thermal pressure to hold off the solar wind in the ionopause at Mars, with only 13% unmagnetized ionopauses observed over a 11-year period. We also find that the ionopause altitude decreases as the normal component of the solar wind dynamic pressure increases. Moreover, our results show that the ionopause thickness at Mars is mainly determined by the ion gyromotion and equivalent to about 5.7 ion gyroradii.

Solar Wind Interaction and Pressure Balance at the Dayside Ionopause of Mars

F. Chu[1], F. Duru[2], Z. Girazian[3], R. Ramstad[4], J. Halekas[3], D. A. Gurnett[3], Xin Cao[3], and A. J. Kopf[3]

[1]Physics Division, Los Alamos National Laboratory, Los Alamos, NM, USA
[2]Department of Physics, Coe College, Cedar Rapids, IA, USA
[3]Department of Physics and Astronomy, University of Iowa, Iowa City, IA, USA
[4]Laboratory for Atmospheric and Space Physics, University of Colorado Boulder, Boulder, CO, USA

Key Points:

- 13% of the ionopauses at Mars are unmagnetized; the unmagnetized ionopauses occur 65% at Venus at solar maximum and 52% at solar minimum
- The ionopause altitude decreases with the solar wind dynamic pressure at Mars, similar to the altitude variation of the ionopauses at Venus
- The ionopause thickness at Mars is mainly determined by the ion gyromotion and equivalent to about 5.7 ion gyroradii

Corresponding author: F. Chu, fchu@lanl.gov

Abstract

Due to the lower ionospheric thermal pressure and existence of the crustal magnetism at Mars, the Martian ionopause is expected to behave differently from the ionopause at Venus. We study the solar wind interaction and pressure balance at the ionopause of Mars using both in situ and remote sounding measurements from the MARSIS (Mars Advanced Radar for Subsurface and Ionosphere Sounding) instrument on the Mars Express orbiter. We show that the magnetic pressure usually dominates the thermal pressure to hold off the solar wind in the ionopause at Mars, with only 13% unmagnetized ionopauses observed over a 11-year period. We also find that the ionopause altitude decreases as the normal component of the solar wind dynamic pressure increases. Moreover, our results show that the ionopause thickness at Mars is mainly determined by the ion gyromotion and equivalent to about 5.7 ion gyroradii.

Plain Language Summary

An ionopause is a sharp decrease in the plasma density at the top of the ionosphere. It was found to be a common feature at Venus, where its variability is well constrained by observations from the Pioneer Venus Orbiter (PVO). Past studies have shown that there are many similarities between the ionopauses at Mars and Venus. However, because the thermal pressure of the ionosphere at Mars is lower than that of Venus, the Martian ionopause is also thought to behave differently from the ionopause at Venus. We study the pressure configuration inside the ionopause at Mars and find that most of the time the magnetic pressure is greater than the thermal pressure. We also find that higher solar wind pressure pushes the ionopause downward at Mars. Moreover, we show that the thickness of the ionopauses at Mars equals a few radii of ion circular motion in the magnetic field. Our results provide insight to the process that controls the formation of the ionopause at Mars.

1 Introduction

Since Mars does not possess a strong global intrinsic magnetic field, the incident solar wind plasma and interplanetary magnetic field interacts inductively with its upper atmosphere and highly conductive ionosphere. This interaction induces currents that produce a magnetic barrier to prevent the solar wind from further penetrating into the atmosphere (Ramstad et al., 2020), resulting in the formation of several plasma boundaries around Mars, such as the magnetic pileup boundary (Crider et al., 2002; Bertucci et al., 2004, 2005), photoelectron boundary (Garnier et al., 2017; Q. Han et al., 2019), and the ionopause (Nagy et al., 2004; X. Han et al., 2014).

The Martian ionopause is a feature identified as a steep gradient in electron density at the topside of the ionosphere. It is a tangential discontinuity that marks the transition from the hot plasma in the induced magnetosphere to the cold, dense ionospheric plasma. When the solar wind flows around Mars, it exerts its dynamic pressure indirectly on the ionosphere through the magnetosheath and magnetic pileup region. Therefore, as the ionospheric thermal pressure decreases sharply across the ionopause, a magnetic pressure from an intrinsic or induced field is required to maintain a steady state of the ionosphere (Holmberg et al., 2019; Sánchez-Cano et al., 2020).

Since Venus also lacks a global-scale magnetic field and its upper atmosphere interacts directly with the solar wind, the ionopauses at Venus and Mars are similar in many aspects. For example, solar wind conditions can heavily influence the dynamics of the ionopauses at both planets (Phillips et al., 1985; Sánchez-Cano et al., 2020). Moreover, the altitudes of Venusian and Martian ionopauses both vary over the solar cycle as a result of the periodic effects of solar EUV on the ionospheric thermal pressure (Kliore & Luhmann, 1991; Duru et al., 2020). Thanks to the Pioneer Venus Orbiter (PVO) mission, the studies of the ionopause at Venus have provided many deep insights that can be applied to understanding the formation of the ionopause at Mars.

On the other hand, because of the lower ionospheric thermal pressure and presence of the highly-localized crustal magnetic fields at Mars, the behavior of the Martian ionopause is also quite different from that at Venus. As the peak thermal pressure in the ionosphere at Mars rarely exceeds the solar wind dynamic pressure, unlike Venus, the Martian ionosphere is often found to be magnetized (Nagy et al., 2004). The magnetic pressure, therefore, plays a more important role in standing off the solar wind ram pressure in the ionopause at Mars. In addition, Chu et al. (2019) found that the strong crustal fields act as minimagnetospheres that prevent the ionopause from forming.

In the past, a number of studies have been dedicated to the investigation of the dependence of the ionopause altitude on solar zenith angle (SZA) and solar extreme ultraviolet (EUV) flux, as well as the effects of the crustal magnetic fields on the formation of the ionopause at Mars (Vogt et al., 2015; Chu et al., 2019; Duru et al., 2020). In this paper, we take advantage of both in situ and remote sounding measurements from the Mars Advanced Radar for Subsurface and Ionosphere Sounding (MARSIS) instrument on board the Mars Express (MEX) spacecraft to study the pressure configuration and balance in the Martian ionopause. We also report for the first time on the mechanisms that control the thickness of the ionopause at Mars. The paper is organized as follows: section 2 gives a description of the ionopause observations from the MARSIS instrument, section 3 explains the pressure terms used in the analysis, section 4 presents the results, and section 5 gives conclusions of the paper.

2 Ionopause Observations

The MARSIS instrument on board the Mars Express spacecraft is a low-frequency radar sounder designed to perform both subsurface and ionospheric soundings (Picardi et al., 2004). In this study, the ionopause is detected by MARSIS using two different techniques – remote radar sounding and in situ measurements.

To obtain the plasma density profile of the ionosphere, MARSIS sends a short radio pulse from 0.1 to 5.4 MHz and detects any return echoes that are reflected off the ionosphere (Gurnett et al., 2005). The reflection occurs at the point where the frequency of the electromagnetic wave is below the local electron plasma frequency $f_{\mathrm{p}} = 8980\sqrt{n_{\mathrm{e}}}$ Hz, where n_{e} is the electron density in cm^{-3} (Gurnett & Bhattacharjee, 2005). By measuring the time delay Δt between the transmission of the pulse and the time that the echo is received, the apparent altitude of the reflection point can be expressed as $h = h_{\mathrm{MEX}} - c\Delta t/2$, where h_{MEX} is the spacecraft altitude and c is the speed of light. The term apparent altitude refers to the scale that has not been corrected for dispersion of the radar pulses that propagate in a plasma; however, in our situation where the dispersion effects are small, the apparent altitude is very close to the real altitude. The detailed discussion about the apparent altitude can be found in Chu et al. (2019). MARSIS remote sounding data are displayed in ionograms, the intensity of the return echoes as a function of frequency and time delay. An example of an ionospheric sounding ionogram is presented in Figure 1a, where the ionopause can be seen as a horizontal line at frequencies below 0.4 MHz, representing a steep density change over a short vertical distance (Chu et al., 2019).

The ionopause can also be identified through MARSIS in situ density measurements (Duru et al., 2009). When MARSIS sounds the ionosphere, intense electrostatic electron plasma oscillations can be excited at the local electron plasma frequency surrounding the spacecraft (Gurnett et al., 2008). When these oscillations are picked up by MARSIS, the received waveforms are often severely clipped, resulting in closely spaced vertical harmonic lines in the low frequency region of the ionogram as shown in Figure 1b. The local electron density can then be calculated from the harmonic spacing Δf (in the units of Hz) using $n_\mathrm{e} = (\Delta f/8980)^2$ cm^{-3}. As MEX enters or exits the topside ionosphere, one can identify the ionopause by looking for the signature of steep density gradient in the local electron density profile.

3 Pressure Terms at the Ionopause

To investigate the solar wind interaction and pressure balance at the ionopause, we need to evaluate the pressures that are exerted on the ionopause. In this study specifically, we consider three different pressure terms, the thermal pressure of the ionosphere, magnetic pressure, and the solar wind dynamic pressure.

3.1 Ionospheric Thermal Pressure

Based on MARSIS in situ electron density measurements, the thermal pressure of the ionosphere can be estimated as

$$P_\mathrm{th} = n_\mathrm{i} k T_\mathrm{i} + n_\mathrm{e} k T_\mathrm{e} \approx 2 n_\mathrm{e} k T_\mathrm{e}, \tag{1}$$

where T_i and T_e are the ion and electron temperature, respectively, n_i is the ion density ($n_\mathrm{i} \approx n_\mathrm{e}$), and k is the Boltzmann constant. Here we assume equal ion and electron temperature $T_\mathrm{i} \approx T_\mathrm{e}$ as the first order approximation for at least up to 350 km (Hanson & Mantas, 1988; Matta et al., 2014). We also use a fixed representation of the T_e profile that does not account for potential SZA, latitude, seasonal, or solar activity variations (Ergun et al., 2015; Pilinski et al., 2019).

3.2 Magnetic Pressure in the Ionosphere

In addition to the vertical electron plasma oscillation harmonics discussed in section 2, another commonly found feature in many MARSIS ionograms is a series of equally spaced horizontal echoes in time at frequencies below 1 MHz, as shown in Figure 1b. When

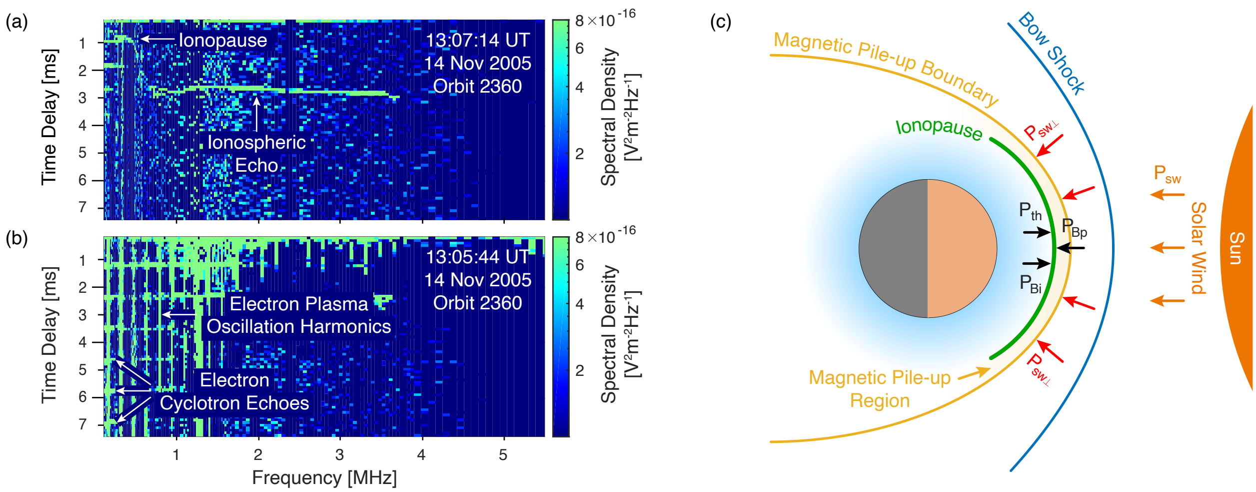

Figure 1. (a) An example of the color-coded MARSIS ionogram from the orbit 2360 on 14 November 2005. The ionopause can be seen as a horizontal line at frequencies below 0.4 MHz. (b) Another ionogram from the same orbit showing the features of the electron plasma oscillation harmonics and electron cyclotron echoes. (c) Schematic illustration of the pressure terms at the ionopause. P_{th} is the ionospheric thermal pressure, P_{Bi} is the magnetic pressure in the ionosphere, P_{Bp} is the magnetic pressure in the magnetic pileup region, and P_{sw} is the solar wind dynamic pressure.

electrons near the antenna are accelerated by the strong electric fields during each transmission cycle, they go through cyclotron motions in the local magnetic field and periodically return to the vicinity of the antenna, causing the electron cyclotron echoes to appear in the ionogram (Gurnett et al., 2005). The repetition rate of these echoes is equal to the local electron cyclotron frequency

$$f_{\mathrm{c}} = \frac{Be}{2\pi m_{\mathrm{e}}}, \tag{2}$$

where B is the magnetic field strength, e is the electron charge, and m_{e} is the electron mass. Since MEX is not equipped with a magnetometer, these electron cyclotron echoes provide the only method to measure the local magnetic field.

As the peak thermal pressure in the Mars ionosphere rarely exceeds the solar wind dynamic pressure, the dayside ionosphere is often found to be magnetized in order to stand off the solar wind (Zhang et al., 1990; Nagy et al., 2004). Over the regions away from the strong crustal magnetism, we can assume that the magnetic field is approximately tangential to the ionopause. Thus, the magnetic pressure in the ionosphere normal to the ionopause can be estimated to the first order as

$$P_{\mathrm{Bi}} = \frac{B^2}{2\mu_0}, \tag{3}$$

where μ_0 is the permeability of free space.

3.3 Solar Wind Dynamic Pressure

Since MEX does not directly measure the properties of the solar wind, the solar wind dynamic pressure P_{sw} is estimated based on the ASPERA (Analyzer of Space Plasma and Energetic Atoms) solar wind moments, which are calculated from averaged proton distributions collected over the inbound/outbound segments of MEX outside the bow shock (Barabash et al., 2006; Ramstad et al., 2015, 2017)

$$P_{\mathrm{sw}} = n_{\mathrm{p}} m_{\mathrm{p}} v_{\mathrm{p}}^2, \tag{4}$$

where n_{p} is the proton density, m_{p} is the proton mass, and v_{p} is the speed of the solar wind.

Note that the normal component of the solar wind ram pressure is not directly exerted on the ionopause; rather it is first converted to thermal pressure in the magnetosheath, then to magnetic pressure in the pileup region. The normal component of the solar wind dynamic pressure can be written as

$$P_{\mathrm{sw}\perp} = \alpha P_{\mathrm{sw}} \cos^2\theta, \tag{5}$$

where θ is the angle between the magnetic pileup boundary normal and the flow direction of the upstream solar wind, and $\alpha \approx 0.88$ is the proportionality constant (Crider et al., 2003). For lower solar zenith angles, θ can be approximately replaced by SZA. At higher SZAs, however, this approximation breaks down because the curvature of the obstacle must be accounted. The pressure values used in the study are the closest ones to the time when the ionopause is observed within 6 hours.

A schematic illustration of the three pressure terms P_{th}, P_{Bi}, and P_{sw} is shown in Figure 1c. In theory, a pressure balance across the ionopause requires

$$P_{\mathrm{th}} + P_{\mathrm{Bi}} = P_{\mathrm{sw}\perp}. \tag{6}$$

In other words, the ionospheric thermal pressure and magnetic pressure should stand off the normal component of the solar wind dynamic pressure. A detailed examination of this pressure balance relation will be presented in section 4.

4 Results

In this study, we utilize both MARSIS in situ (79 detections) and remote sounding (1,791 detections) measurements, excluding crustal magnetic field regions, to study the pressure balance in Martian ionopauses and their interactions with the solar wind. The descriptions of these datasets can be found in Chu et al. (2019) and Duru et al. (2020). We first compare the pressure configuration in the ionopause at Venus and Mars, and then investigate the role of the solar wind in the formation of the Martian ionopause. Finally, we study the dependence of the ionopause thickness at Mars on altitude and magnetic field strength.

4.1 Comparison of Pressure Configuration in Ionopauses at Venus and Mars

The maximum ionospheric thermal pressure at Venus often exceeds the solar wind dynamic pressure (Zhang & Luhmann, 1992). The thermal pressure of the ionosphere, therefore, plays a dominant role in the pressure balance underneath the ionopause. Figure 2a shows a typical example of the pressure configuration in the ionopause at Venus

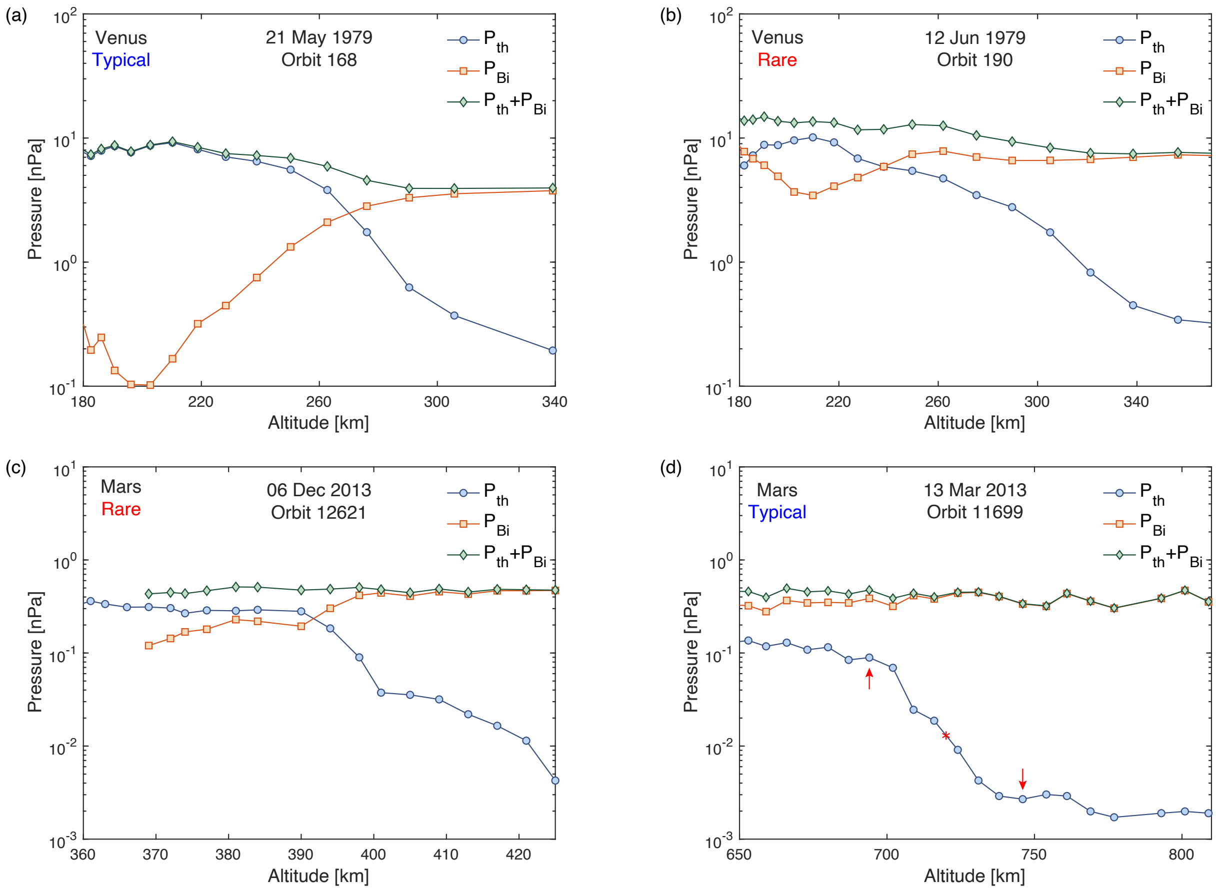

Figure 2. (a)–(b) Thermal pressure and magnetic pressure profiles in the Venusian ionopause as a function of the altitude. The data shown here are based on the in situ measurements from the Pioneer Venus Orbiter's Electron Temperature Probe. A typical example of the pressure configuration is shown in (a) and a rare case is shown in (b). (c)–(d) Thermal pressure and magnetic pressure profiles in the Martian ionopause as a function of the altitude. A rare, Venusian-like example of the pressure configuration is shown in (c) and a typical case is shown in (d). As an example, the red arrows in (d) mark the ionopause thickness and the red star represents the location where the total pressure $P_{\rm tot} = P_{\rm th} + P_{\rm Bi}$ is measured.

(Orbit 168 on 21 May 1979) during solar maximum. Inside the ionopause, as the thermal pressure decreases, the magnetic pressure is forced to increase to maintain the pressure balance. There are some rare occasions shown in Figure 2b (Orbit 190 on 12 June 1979), where the magnetic pressure underneath the ionopause is around the same order of magnitude as the thermal pressure. In such cases, both of the pressure terms are equally important in balancing the solar wind dynamic pressure above the ionopause.

Due to the lower ionospheric thermal pressure at Mars, the behavior of the Martian ionopause is expected to be different from the ionopause at Venus. Figure 2c shows a rare, Venusian-like (typical pressure configuration at Venus) pressure configuration in the Martian ionopause, only found in 13% of all the cases over a 11-year period. In contrast, the similar pressure configuration at Venus shown in Figure 2a is observed at least 65% at solar maximum (Luhmann et al., 1980; Elphic et al., 1981) and $\sim$ 52% at solar minimum (Angsmann et al., 2011). Figure 2d shows a typical pressure configuration in the ionopause at Mars, where the magnetic pressure is clearly seen to play a dominant roll in the pressure balance anywhere in the ionopause.

4.2 Influence of Solar Wind on Martian Ionopause

At Venus, the dynamic behavior of the ionopause is strongly affected by the upstream solar wind conditions. In our previous study, we showed how crustal magnetism and solar extreme ultraviolet flux control the ionopause formation at Mars (Chu et al., 2019). Here, we examine the influence of the solar wind dynamic pressure on ionopause apparent altitude at Mars based on 1,791 ionopause detections (SZA $< 65°$) obtained using the MARSIS remote sounding technique (Figure 3a). Despite a strong scattering of the data points in Figure 3a, likely due to the variations of seasons and solar extreme ultraviolet (EUV) flux (more plots showing the distribution in season, EUV flux, latitude, and SZA can be found in the supporting information), we find that the ionopause altitude decreases with the normal component of the solar wind dynamic pressure by 131 ± 50 km/nPa. Similar ionopause altitude variation with the solar wind dynamic pressure was also observed at Venus by PVO (Brace et al., 1980). The trend shown in Figure 3a, however, was not found in Vogt et al. (2015), possibly because they had a smaller data set or a different detection method. These solar wind effects are also observed in other plasma boundaries at Mars (Edberg et al., 2009; Withers et al., 2016; Garnier et al., 2017; Halekas et al., 2018; Girazian, Halekas, et al., 2019).

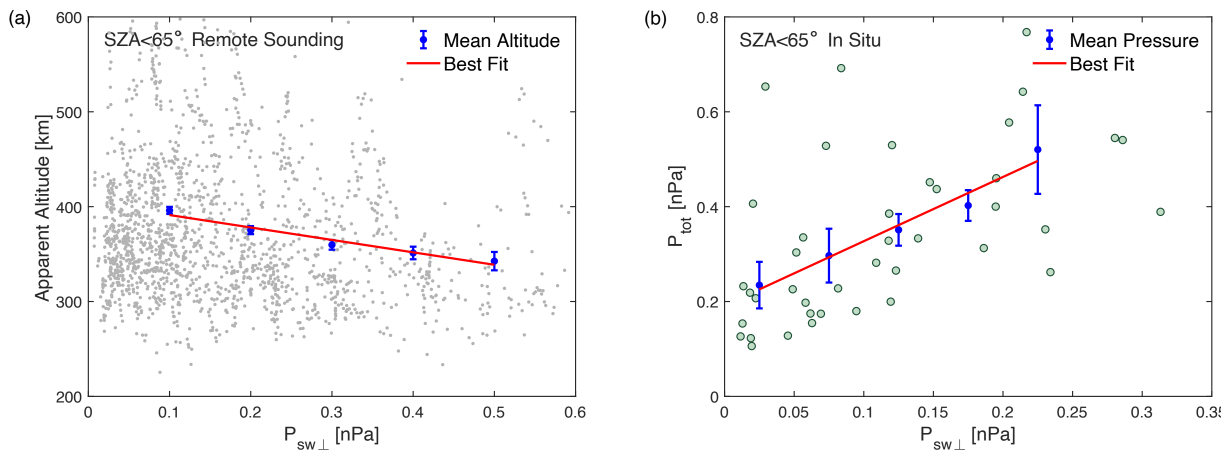

Figure 3. (a) Scatter plot of the ionopause apparent altitude (SZA $<$ 65°) as a function of the normal component of the solar wind dynamic pressure at Mars. The ionopause data are collected using the MARSIS remote sounding technique. The mean ionopause altitude averaged over each 0.1 nPa bin is shown in blue dots. (b) Correlation between the total ionopause pressure (SZA $<$ 65°) and normal component of the solar wind dynamic pressure at Mars. The mean ionopause pressure for each 0.05 nPa bin is shown in blue dots. Error bars in (a)–(b) represent the standard deviation of the mean ($\sigma/\sqrt{N}$, σ standard deviation and N number of data points in each bin). SZA=solar zenith angle.

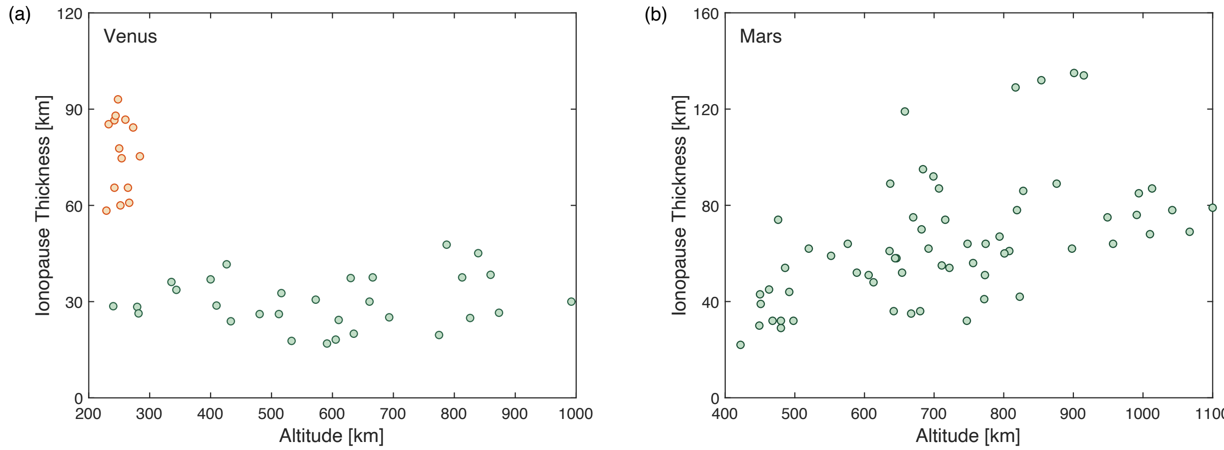

Figure 4. (a) Ionopause thickness as a function of altitude at Venus, reproduced from Figure 6 in Elphic et al. (1981). The orange and green dots mark the ionopauses forming at low and high altitudes, respectively. (b) Ionopause thickness as a function of altitude at Mars, based on the MARSIS in situ measurements.

To test the theory for pressure balance in the ionopause, we plot the total pressure inside the ionopause ($P_{\rm tot} = P_{\rm th} + P_{\rm Bi}$, the location of which is measured is shown as an example in Figure 2d) as a function of the normal component of the solar wind dynamic pressure for SZA $< 65°$ in Figure 3b. We then perform a linear fit (least squares) for the average pressure in each pressure bin using the formula $P_{\rm tot} = aP_{\rm sw\perp} + b$, and find that $a = 1.36 \pm 0.44$. The slope close to unity indicates that the total pressure $P_{\rm tot}$ inside the ionopause on average balances the normal component of the solar wind dynamic pressure $P_{\rm sw\perp}$, consistent with the similar test based on the simultaneous measurements by ASPERA and MAVEN (Mars Atmosphere and Volatile Evolution) in Sánchez-Cano et al. (2020). Additionally, we find that $b = 0.19 \pm 0.06$ nPa, a small offset between $P_{\rm tot}$ and $P_{\rm sw\perp}$, which suggests that $P_{\rm tot}$ may slightly exceed $P_{\rm sw\perp}$ at the location where the ionopause forms, in agreement with the results shown in Holmberg et al. (2019).

4.3 Dependence of Ionopause Thickness on Altitude

We identify the thickness of a Martian ionopause as the length scale of the steep change in ionospheric plasma density greater than $\Delta n/n > 0.1$ within a single MARSIS frequency sweep period (7.54 s), equivalent to a minimum density gradient of ~ 2 cm^{-3}/km. An example illustrating the ionopause thickness is shown in Figure 2d. Since the ionopause is essentially a current sheet induced to shield the solar wind magnetic field from penetrating into the upper ionosphere, the thickness of this boundary layer is expected to be on the order of the ion gyroradius scale (Cravens & Shinagawa, 1991). However, there are also other factors that can affect the ionopause thickness, such as diffusion (Elphic et al., 1981).

At Venus, past observations from PVO showed that the ionopauses can be mainly grouped into two classes based on the mechanisms that determine their thickness – the thick ionopauses (thickness $>$ 60 km) at low altitudes and thinner ones at high altitudes (Elphic et al., 1981). The PVO measurements of the ionopause thickness as a function of altitude are shown in Figure 4a (reproduced from Figure 6 in Elphic et al., 1981). When the ionopause forms at low altitudes (colored in orange), due to relatively high ionospheric density, the ion coulomb collision rate usually dominates the ion gyrofrequency in this boundary layer, making diffusive broadening an important process in determining the ionopause thickness. However, as the altitude increases, the coulomb collision rate falls off rapidly, causing the thickness of the ionopause forming in high altitudes (colored in green) simply proportional to the ion gyroradius. Since the variation of the ion temperature is small above 300 km, thus the thickness of these ionopauses is also inversely proportional to the magnetic field strength (Miller et al., 1980). Figure 5a shows the PVO measurements of the ionopause thickness as a function of the field strength (reproduced from Figure 5 in Elphic et al., 1981). If we rewrite the ion gyroradius as $\rho_\mathrm{i} = \sqrt{m_\mathrm{i} k T_\mathrm{i}}/Be$, where m_i is the ion mass, by fitting the thickness of the ionopauses at high altitudes (colored in green) with formula $d = \gamma\rho_i$ and assuming the temperature of O^+ ions $T_\mathrm{i} \approx$ 3000 K, we find that on average the ionopause thickness is about $\gamma = 5.3 \pm 0.9$ ion gyroradii at Venus (Elphic et al., 1981).

At Mars, however, the ionospheric density is much smaller than that at Venus. Previous studies have shown that the ion coulomb collision rate is only comparable to the ion gyrofrequency in the ionospheric dynamo region that lies between 100 and 250 km in altitude, well below that of the ionopause (Withers, 2008; Opgenoorth et al., 2010). Therefore, in contrast to the two main mechanisms that affect the thickness of Venusian ionopauses at low and high altitudes, the ion gyroradius scale becomes the most important factor that determines the ionopause thickness at Mars. Figure 4b shows the ionopause thickness as a function of altitude based on the MARSIS in situ measurements. In general, we find that the ionopause thickness increases with altitude at Mars due to lower

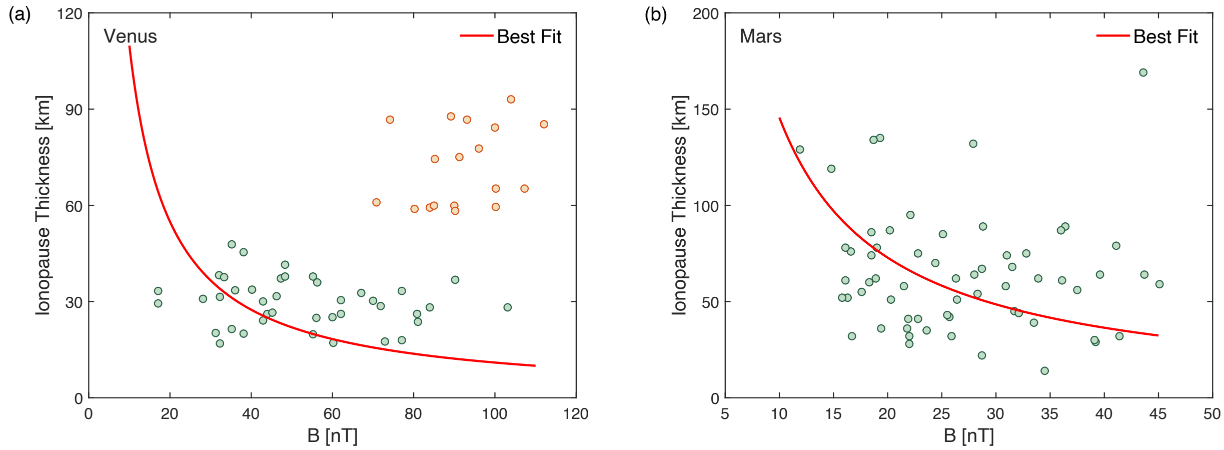

Figure 5. (a) Ionopause thickness as a function of magnetic field strength at Venus, reproduced from Figure 5 in Elphic et al. (1981). Same as Figure 4a, the orange and green dots represent the ionopauses forming at low and high altitudes, respectively. (b) Ionopause thickness as a function of magnetic field strength at Mars, based on the MARSIS in situ measurements. The red curves in (a) and (b) represent the best fit of the green dots with the formula $d = \gamma\sqrt{m_\mathrm{i} k T_\mathrm{i}}/Be \propto 1/B$.

magnetic field strength at higher altitudes (Holmberg et al., 2019). Figure 5b shows the ionopause thickness as a function of the field strength. If we assume the topside ionospheric composition is about 50% O^+ ions and 50% O_2^+ ions, and $T_\mathrm{i} \approx T_\mathrm{e} \approx 3000$ K, by repeating the same procedure as in Figure 5a, we find that the ionopause at Mars has a thickness of 5.7±0.8 ion gyroradii, comparable to 5.3 ion gyroradii at Venus (Girazian, Mahaffy, et al., 2019).

5 Conclusions

In conclusion, we have investigated the solar wind interaction and pressure balance at the dayside ionopause of Mars using both in situ and remote sounding measurements from the MARSIS instrument. We have found that most of the time the magnetic pressure dominates the thermal pressure to hold off the solar wind in the ionopause at Mars. Only about 13% of the ionopauses that we examined over a 11-year period are unmagnetized, whereas the unmagnetized ionopauses account for at least 52% at Venus. Additionally, our analysis has shown that the ionopause altitude decreases as the solar wind dynamic pressure increases at Mars, similar to the altitude variation of the ionopauses at Venus. Finally, we have shown for the first time that the thickness of the ionopauses at Mars is mainly determined by the ion gyromotion, much alike the ionopauses forming in high altitudes at Venus. The ionopauses at Mars are found to have a thickness of about 5.7 ion gyroradii, surprisingly close to the ionopause thickness of 5.3 ion gyroradii at Venus.

Acknowledgments

This work was supported by NASA through Contract No. 1560641 with the Jet Propulsion Laboratory. All of the MARSIS and PVO data used in this paper are publicly available through the NASA Planetary Data System (PDS). The solar wind moments are archived on ESA's Planetary Science Archive (`https://archives.esac.esa.int/psa/pub/mirror/MARS-EXPRESS/296ASPERA-3/MEX-SUN-ASPERA3-4-SWM-V1.0/#!Table%20View/ASPERA-3=instrument`).

References

Angsmann, A., Fränz, M., Dubinin, E., Woch, J., Barabash, S., Zhang, T. L., & Motschmann, U. (2011, March). Magnetic states of the ionosphere of Venus observed by Venus Express. *Planetary and Space Science*, *59*(4), 327–337. doi: 10.1016/j.pss.2010.12.004

Barabash, S., Lundin, R., Andersson, H., Brinkfeldt, K., Grigoriev, A., Gunell, H., … Thocaven, J.-J. (2006, October). The Analyzer of Space Plasmas and Energetic Atoms (ASPERA-3) for the Mars Express Mission. *Space Sci Rev*, *126*(1), 113–164. doi: 10.1007/s11214-006-9124-8

Bertucci, C., Mazelle, C., Acuña, M. H., Russell, C. T., & Slavin, J. A. (2005). Structure of the magnetic pileup boundary at Mars and Venus. *J. Geophys. Res. Space Phys.*, *110*(A1). doi: 10.1029/2004JA010592

Bertucci, C., Mazelle, C., Crider, D. H., Mitchell, D. L., Sauer, K., Acuña, M. H., … Winterhalter, D. (2004, January). MGS MAG/ER observations at the magnetic pileup boundary of Mars: Draping enhancement and low frequency waves. *Advances in Space Research*, *33*(11), 1938–1944. doi: 10.1016/j.asr.2003.04.054

Brace, L. H., Theis, R. F., Hoegy, W. R., Wolfe, J. H., Mihalov, J. D., Russell, C. T., … Nagy, A. F. (1980). The dynamic behavior of the Venus ionosphere in response to solar wind interactions. *J. Geophys. Res. Space Phys.*, *85*(A13), 7663–7678. doi: 10.1029/JA085iA13p07663

Chu, F., Girazian, Z., Gurnett, D. A., Morgan, D. D., Halekas, J., Kopf, A. J., ... Duru, F. (2019). The Effects of Crustal Magnetic Fields and Solar EUV Flux on Ionopause Formation at Mars. *Geophys. Res. Lett.*, *46*(17-18), 10257–10266. doi: 10.1029/2019GL083499

Cravens, T. E., & Shinagawa, H. (1991). The ionopause current layer at Venus. *J. Geophys. Res. Space Phys.*, *96*(A7), 11119–11131. doi: 10.1029/91JA00674

Crider, D. H., Acuña, M. H., Connerney, J. E. P., Vignes, D., Ness, N. F., Krymskii, A. M., ... Winterhalter, D. (2002). Observations of the latitude dependence of the location of the martian magnetic pileup boundary. *Geophys. Res. Lett.*, *29*(8), 11-1-11-4. doi: 10.1029/2001GL013860

Crider, D. H., Vignes, D., Krymskii, A. M., Breus, T. K., Ness, N. F., Mitchell, D. L., ... Acuña, M. H. (2003). A proxy for determining solar wind dynamic pressure at Mars using Mars Global Surveyor data. *J. Geophys. Res. Space Phys.*, *108*(A12). doi: 10.1029/2003JA009875

Duru, F., Baker, N., De Boer, M., Chamberlain, A., Verchimak, R., Morgan, D. D., ... Kopf, A. (2020, May). Martian Ionopause Boundary: Coincidence With Photoelectron Boundary and Response to Internal and External Drivers. *Journal of Geophysical Research: Space Physics*, *125*(5), e2019JA027409. doi: 10.1029/2019JA027409

Duru, F., Gurnett, D. A., Frahm, R. A., Winningham, J. D., Morgan, D. D., & Howes, G. G. (2009). Steep, transient density gradients in the Martian ionosphere similar to the ionopause at Venus. *J. Geophys. Res. Space Phys.*, *114*(A12). doi: 10.1029/2009JA014711

Edberg, N. J. T., Brain, D. A., Lester, M., Cowley, S. W. H., Modolo, R., Fränz, M., & Barabash, S. (2009, September). Plasma boundary variability at Mars as observed by Mars Global Surveyor and Mars Express. *Ann. Geophys.*, *27*(9), 3537–3550. doi: 10.5194/angeo-27-3537-2009

Elphic, R. C., Russell, C. T., Luhmann, J. G., Scarf, F. L., & Brace, L. H. (1981). The Venus ionopause current sheet: Thickness length scale and controlling factors. *J. Geophys. Res. Space Phys.*, *86*(A13), 11430–11438. doi: 10.1029/JA086iA13p11430

Ergun, R. E., Morooka, M. W., Andersson, L. A., Fowler, C. M., Delory, G. T., Andrews, D. J., … Jakosky, B. M. (2015). Dayside electron temperature and density profiles at Mars: First results from the MAVEN Langmuir probe and waves instrument. *Geophys. Res. Lett.*, *42*(21), 8846–8853. doi: 10.1002/2015GL065280

Garnier, P., Steckiewicz, M., Mazelle, C., Xu, S., Mitchell, D., Holmberg, M. K. G., … Jakosky, B. M. (2017). The Martian Photoelectron Boundary as Seen by MAVEN. *J. Geophys. Res. Space Phys.*, *122*(10), 10,472–10,485. doi: 10.1002/2017JA024497

Girazian, Z., Halekas, J., Morgan, D. D., Kopf, A. J., Gurnett, D. A., & Chu, F. (2019). The Effects of Solar Wind Dynamic Pressure on the Structure of the Topside Ionosphere of Mars. *Geophys. Res. Lett.*, *46*(15), 8652–8662. doi: 10.1029/2019GL083643

Girazian, Z., Mahaffy, P., Lee, Y., & Thiemann, E. M. B. (2019, April). Seasonal, Solar Zenith Angle, and Solar Flux Variations of O+ in the Topside Ionosphere of Mars. *Journal of Geophysical Research: Space Physics*, *124*(4), 3125–3138. doi: 10.1029/2018JA026086

Gurnett, D. A., & Bhattacharjee, A. (2005). *Introduction to Plasma Physics: With Space and Laboratory Applications*. Cambridge University Press.

Gurnett, D. A., Huff, R. L., Morgan, D. D., Persoon, A. M., Averkamp, T. F., Kirchner, D. L., … Picardi, G. (2008, January). An overview of radar soundings of the martian ionosphere from the Mars Express spacecraft. *Advances in Space Research*, *41*(9), 1335–1346. doi: 10.1016/j.asr.2007.01.062

Gurnett, D. A., Kirchner, D. L., Huff, R. L., Morgan, D. D., Persoon, A. M., Averkamp, T. F., … Picardi, G. (2005, December). Radar Soundings of the Ionosphere of Mars. *Science*, *310*(5756), 1929–1933. doi: 10.1126/science.1121868

Halekas, J. S., McFadden, J. P., Brain, D. A., Luhmann, J. G., DiBraccio, G. A., Connerney, J. E. P., … Jakosky, B. M. (2018, October). Structure and Variability of the Martian Ion Composition Boundary Layer. *Journal of Geophysical Research: Space Physics*, *123*(10), 8439–8458. doi: 10.1029/2018JA025866

Han, Q., Fan, K., Cui, J., Wei, Y., Fraenz, M., Dubinin, E., … Connerney, J. (2019, October). The Relationship Between Photoelectron Boundary and Steep Electron Density Gradient on Mars: MAVEN Observations. *J. Geophys. Res. Space Physics*, *124*(10), 8015–8022. doi: 10.1029/2019JA026739

Han, X., Fraenz, M., Dubinin, E., Wei, Y., Andrews, D. J., Wan, W., … Barabash, S. (2014). Discrepancy between ionopause and photoelectron boundary determined from Mars Express measurements. *Geophys. Res. Lett.*, *41*(23), 8221–8227. doi: 10.1002/2014GL062287

Hanson, W. B., & Mantas, G. P. (1988, July). Viking electron temperature measurements: Evidence for a magnetic field in the Martian ionosphere. *Journal of Geophysical Research: Space Physics*, *93*(A7), 7538–7544. doi: 10.1029/JA093iA07p07538

Holmberg, M. K. G., André, N., Garnier, P., Modolo, R., Andersson, L., Halekas, J., … Mitchell, D. L. (2019). MAVEN and MEX Multi-instrument Study of the Dayside of the Martian Induced Magnetospheric Structure Revealed by Pressure Analyses. *J. Geophys. Res. Space Phys.*, *124*(11), 8564–8589. doi: 10.1029/2019JA026954

Kliore, A. J., & Luhmann, J. G. (1991). Solar cycle effects on the structure of the electron density profiles in the dayside ionosphere of Venus. *J. Geophys. Res. Space Phys.*, *96*(A12), 21281–21289. doi: 10.1029/91JA01829

Luhmann, J. G., Elphic, R. C., Russell, C. T., Mihalov, J. D., & Wolfe, J. H. (1980, November). Observations of large scale steady magnetic fields in the dayside Venus ionosphere. *Geophysical Research Letters*, *7*(11), 917–920. doi: 10.1029/GL007i011p00917

Matta, M., Galand, M., Moore, L., Mendillo, M., & Withers, P. (2014, January). Numerical simulations of ion and electron temperatures in the ionosphere of Mars: Multiple ions and diurnal variations. *Icarus*, *227*, 78–88. doi: 10.1016/j.icarus.2013.09.006

Miller, K. L., Knudsen, W. C., Spenner, K., Whitten, R. C., & Novak, V. (1980, December). Solar zenith angle dependence of ionospheric ion and electron temperatures and density on Venus. *Journal of Geophysical Research: Space Physics*, *85*(A13), 7759–7764. doi: 10.1029/JA085iA13p07759

Nagy, A. F., Winterhalter, D., Sauer, K., Cravens, T. E., Brecht, S., Mazelle, C., … Trotignon, J. G. (2004, March). The plasma Environment of Mars. *Space Science Reviews*, *111*, 33–114. doi: 10.1023/B:SPAC.0000032718.47512.92

Opgenoorth, H., Dhillon, R., Rosenqvist, L., Lester, M., Edberg, N., Milan, S., ... Brain, D. (2010, August). Day-side ionospheric conductivities at Mars. *Planetary and Space Science*, *58*(10), 1139–1151. doi: 10.1016/j.pss.2010.04.004

Phillips, J., Luhmann, J., & Russell, C. (1985, January). Dependence of Venus ionopause altitude and ionospheric magnetic field on solar wind dynamic pressure. *Advances in Space Research*, *5*(9), 173–176. doi: 10.1016/0273-1177(85)90286-8

Picardi, G., Biccari, D., Seu, R., Plaut, J., Johnson, W. T. K., Jordan, R. L., ... Zampolini, E. (2004, August). MARSIS: Mars Advanced Radar for Subsurface and Ionosphere Sounding. In *Mars Express: The Scientific Payload* (Vol. 1240, pp. 51–69).

Pilinski, M., Andersson, L., Fowler, C., Peterson, W. K., Thiemann, E., & Elrod, M. K. (2019, November). Electron Temperature Response to Solar Forcing in the Low-Latitude Martian Ionosphere. *Journal of Geophysical Research: Planets*, *124*(11), 3082–3094. doi: 10.1029/2019JE006090

Ramstad, R., Barabash, S., Futaana, Y., & Holmström, M. (2017). Solar wind- and EUV-dependent models for the shapes of the Martian plasma boundaries based on Mars Express measurements. *J. Geophys. Res. Space Phys.*, *122*(7), 7279–7290. doi: 10.1002/2017JA024098

Ramstad, R., Barabash, S., Futaana, Y., Nilsson, H., Wang, X.-D., & Holmström, M. (2015). The Martian atmospheric ion escape rate dependence on solar wind and solar EUV conditions: 1. Seven years of Mars Express observations. *J. Geophys. Res. Planets*, *120*(7), 1298–1309. doi: 10.1002/2015JE004816

Ramstad, R., Brain, D. A., Dong, Y., Espley, J., Halekas, J., & Jakosky, B. (2020, October). The global current systems of the Martian induced magnetosphere. *Nat. Astron.*, *4*(10), 979–985. doi: 10.1038/s41550-020-1099-y

Sánchez-Cano, B., Narvaez, C., Lester, M., Mendillo, M., Mayyasi, M., Holmstrom, M., ... Durward, S. (2020). Mars' Ionopause: A Matter of Pressures. *J. Geophys. Res. Space Phys.*, *125*(9), e2020JA028145. doi: 10.1029/2020JA028145

Vogt, M. F., Withers, P., Mahaffy, P. R., Benna, M., Elrod, M. K., Halekas, J. S., ... Jakosky, B. M. (2015). Ionopause-like density gradients in the Martian ionosphere: A first look with MAVEN. *Geophys. Res. Lett.*, *42*(21), 8885–8893. doi: 10.1002/2015GL065269

Withers, P. (2008, July). Theoretical models of ionospheric electrodynamics and plasma transport. *Journal of Geophysical Research: Space Physics*, *113*(A7). doi: 10.1029/2007JA012918

Withers, P., Matta, M., Lester, M., Andrews, D., Edberg, N. J. T., Nilsson, H., ... Witasse, O. (2016, January). The morphology of the topside ionosphere of Mars under different solar wind conditions: Results of a multi-instrument observing campaign by Mars Express in 2010. *Planetary and Space Science*, *120*, 24–34. doi: 10.1016/j.pss.2015.10.013

Zhang, M. H. G., & Luhmann, J. G. (1992). Comparisons of peak ionosphere pressures at Mars and Venus with incident solar wind dynamic Pressure. *J. Geophys. Res. Planets*, *97*(E1), 1017–1025. doi: 10.1029/91JE02721

Zhang, M. H. G., Luhmann, J. G., Kliore, A. J., & Kim, J. (1990). A post-Pioneer Venus reassessment of the Martian dayside ionosphere as observed by radio occultation methods. *J. Geophys. Res. Solid Earth*, *95*(B9), 14829–14839. doi: 10.1029/JB095iB09p14829